X-Ray Tomography with Micrometer Spatial Resolution

C. Raven, A. Snigirev, A. Koch, I. Snigireva, V. Kohn
European Synchrotron Radiation Facility (ESRF)
BP. 220, 38043 Grenoble, France

SPIE, Vol.3149, p.140-148, 1997

ABSTRACT

Three-dimensional computed tomographic images with micrometer resolution were made in phase-contrast mode with high energy X-rays at a third generation synchrotron source. The phase-contrast technique enables one to obtain information not only about the amplitude of the wave field behind the object and thus about the absorption, but also about the refractive index distribution inside the sample. Increasing the X-ray energy from the soft X-ray region (0.2–1 keV) up to 10–60 keV (1.2 to 0.2□ wavelength) simplifies the experimental setup and opens the possibility to study organic samples at room-temperature and under normal pressure conditions. The projection data is recorded with a fast, high-resolution x-ray camera consisting of a 5 μm thin YAG scintillator crystal, a visible light microscope optics and a slow scan 1k□1k CCD camera. The spatial resolution of phase-contrast microtomography is currently limited by the resolution of the X-ray detector to about 1–2 μm. First applications in biology and geophysics are shown.

1 Introduction

Obtaining three-dimensional information on a microscopic scale of a sample without destroying it has long been of high interest in many areas of research. Since the proposition to use synchrotron X-rays to do tomography with smaller objects,[1] different strategies have been pursued to improve the spatial resolution: scanning the sample with a micrometer sized pencil beam,[2] magnifying the X-ray image prior to detection[3,4] or increasing the resolution of the detector.[5,6] In this paper we want to show the feasibility of phase-contrast microtomography by recording a set of phase-contrast images in outline mode with a high-resolution, CCD based X-ray detector.

Phase-contrast imaging, with coherent high-energy X-rays, has become an active area of research with the advent of third generation synchrotron sources like the ESRF.[7,8] It combines a simple experimental setup, consisting of only a monochromator in the upstream beampath, with the advantages of high energy X-rays, namely lower absorbed dosage, less scattering of the beam in air and the possibility to probe thicker samples. Since absorption becomes more and more negligible the higher the X-ray energies are, more sensitive information can be retrieved from the phase shift of the beam inside the object.[9,10]

Fig. 1 represents the principle formation of phase-contrast with coherent X-rays in an in-line holographic setup. By propagation from the object to the detector plane, a fresnel diffraction pattern arises caused by the scattering of the incoming beam at the object. The size of the fringe pattern d depends on the size of the first Fresnel zone $r_{FZ} = \sqrt{\lambda r_1}$, with r_1 the object-to-detector distance and λ the

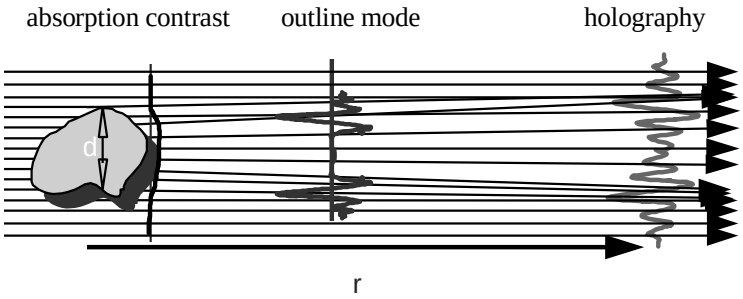

Figure 1: Contrast formation of phase-contrast imaging in an in-line holography setup. By propagating a certain distance from the object to the detector different parts of the wavefront which have experienced different phase shifts can interfere.

wavelength of the incoming X-ray beam. Thus, objects in a beam of 1 □ wavelength show in 10 cm distance only one or two fringes in a region of about 1 μm around the sample edges (outline imaging mode). The outline image resembles in a good approximation the features in the sample, with contrast enhancement at edges and interfaces in the object. The spatial resolution of outline phase-contrast imaging is limited by the detector resolution to about 1 μm for high-resolution X-ray film and, until recently, to several micrometer for online, CCD-based detectors. The resolution of CCD based X-ray detectors was improved considerably by using transparent crystalline luminescent screens to convert the incoming X-rays to detectable visible light. Such a detector, combined with the large depth-of field and the large penetration depth of high-energy X-rays, makes phase-contrast imaging in outline mode directly extendable to computed microtomography. This enables one to obtain three-dimensional information about the sample.[11]

2 Outline Tomography

In computed tomography a large number of images of a sample are taken from different angles of projection. Three-dimensional data can be reconstructed from the projections via a Radon transformation. This connects a set of two-dimensional line-integrals over a function along different paths to the spatial mapping of this function. Using a synchrotron source for tomography simplifies considerably the reconstruction: the incoming beam is practicaly parallel and the monochromaticity avoids artefacts caused by beam hardening in the sample. In standard absorption tomography the logarithm of the normalized projection intensity along a certain projection corresponds to the path integral over the linear attenuation coe□cient along that line.[12] In outline tomography only a quantitative mapping is achieved, i.e. the intensity in the outline-mode images can be regarded as the line-integral over a function which is non-zero only at edges and interfaces in the sample.[11,13] Therefore one finds the three-dimensional location of borders and interfaces in the sample, but not a quantitative mapping of the refractive index (Fig. 2). Gaining information about the location of different components in a sample might be su□cient for a large number of applications. Here we use a filtered backprojection algorithm to reconstruct the cross-sections.

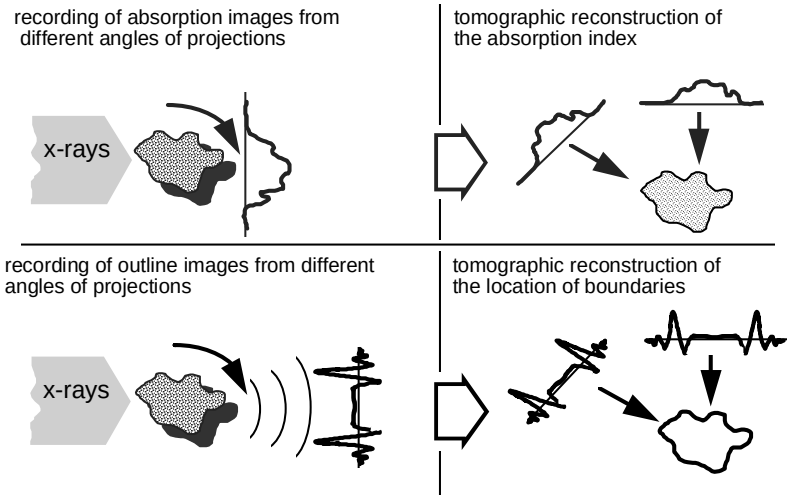

Figure 2: Principle of computed tomography. Several images of different angles of projection are recoreded as input for the reconstruciton algorithm. a) Absorption mode: the images are taken directly behind the object, only the difference in absorption gives rise to contrast. The reconstructed cross-sections show the distribution of the absorption coe□zient inside the sample. b) Outline mode: images are recorded in an in-line holography setup. Contrast is due to absorption and to phase contrast at borders and interfaces in the sample. These borders can then be reconstructed in 3D.

3 Experimental Setup

3.1 Beamline

Experiments were made at different undulator, wiggler and bending magnet beamlines at the ESRF with energies from 8 to 60 keV(wavelength 1.5–0.2 □). The general experimental setup is shown in Fig. 3. The X-ray beam is monochromatized by a Si 111 double crystal Bragg-monochromator. The spatial coherence is given by the source-to-object distance r_0 and by the source size s, i.e. by the vertical size of the electron beam in the storage ring. For a source size s of 50 μm, a source distance r_0 of 50 m and a wavelength of 1 □, the transverse coherence length is about 100 μm.

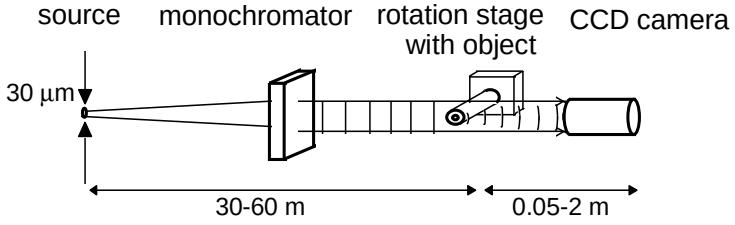

Figure 3: Experimental setup for phase-contrast imaging and phase-contrast tomography at the ESRF. The spatial coherence of the beam is provided by the long source-to-object distance and the small source size. The temporal coherence is given by the monochromator.

The spatial resolution of phase-contrast imaging will eventually be limited by the demagnified source size $s_d = s\frac{r_1}{r_0}$, which will smear out the interference fringes for larger recording distances r_1. For the

above given geometrical values and $r_1 = 10$ cm we find $s_d = 0.1$ μm in vertical and 2 μm in horizontal direction at a undulator beamline, where the source size is 30□600 μm^2. Therefore the sample is rotated around a horizontal axis to have the highest resolution in the plane of reconstruction. Care has to be taken in the choice of the rotation stage; wobble and excentricity of the rotation axis have to be consistent with the demanded resolution. In fact, most of the artefacts in the tomograms are due to mechanical instabilities, introduced by the rotation stage.

3.2 Detector

High-resolution X-ray film (Kodak) provides a resolution of 1 μm and the advantage of a large field of view but with the drawbacks of being an off-line detector, having a non-linear response and a small dynamic range, which make film very impractical for tomographic applications.

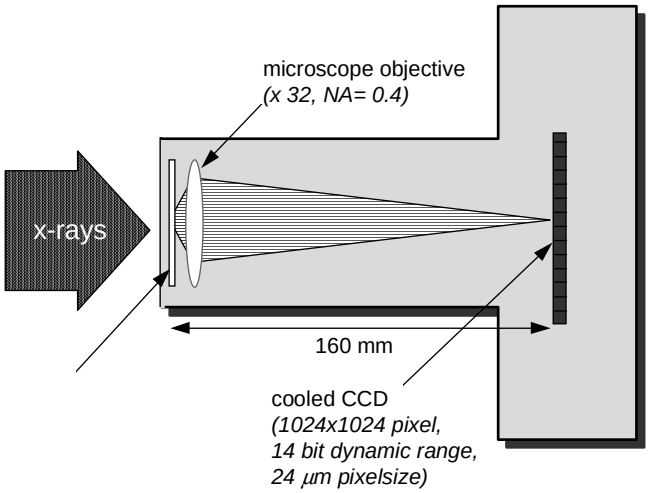

Figure 4: Schematic drawing of the high-resolution X-ray detector. The X-rays are converted to visible light and magnified onto the CCD element. The effective pixelsize is 0.6 μm, the measured spatial resolution (fwhm) is 1.4 μm.

We developed recently[14] a high-resolution on-line X-ray detector, based on a thin scintillator, which is optically magnified onto a CCD chip. This arrangement gives a fast, low noise detector with a linear response function and a theoretical resolution limit given by the diffraction limit of visible light. The practical resolution is limited by the mismatch of the thickness of the scintillator to the focal depth of the microscope objective. That means, not all planes in the scintillator are sharply focused onto the CCD chip, which leads to a blurring of the image. The resolution can therefore only be improved by using thinner scintillators. The current setup consists of a of 5 μm thick YAG:Ce crystalline scintillator on a 1 mm thick YAG substrate, a 40□ magnification microscope optics with a NA of 0.5 and a cooled photometrics 1024□1024 pixel CCD camera with 19 μm pixelsize (Fig.4). The microscope objective is corrected for the thickness of the YAG substrate. By measuring the spot-size of a focussed, submicrometer X-ray beam, we find a spatial resolution of 1.6 μm FWHM at 20 keV.[14] The modulation transfer function (MTF) can be measured directly by recording the hologram of a calibrated object. These holograms have a very wide band of spatial frequencies. Normalizing the recorded frequency spectrum to the calculated spectrum one obtaines directly a value for the MTF of the detector (Fig 5). The exposure time for one image at a bending magnet beamline (with 10^9 ph/sec/mm^2) is of the order of 30 sec, at a high-β undulator beamline (10^{11} ph/sec/mm^2) about 0.5–3 sec. For CCD based X-ray detectors which convert the incoming X-rays to visible light the spatial resolution is limited mainly by three entities: the diffraction limit of light which is for the visible spectrum around 0.5 μm,

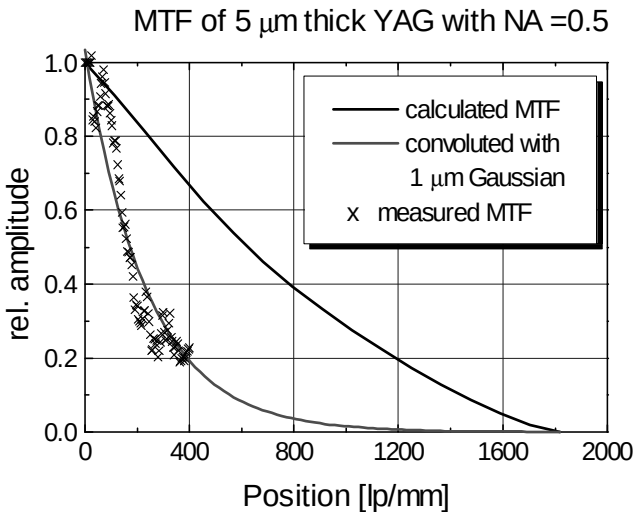

Figure 5: Modulation transfer function (MTF) of the CCD detector with a 5 μm thick YAG scintillator. The theoretical MTF is obtained from the theoretical spectrum of a hologram of a 100 mm thick boron fiber, taking into account spherical aberration, diffraction and focal depth limitations inside the microscope objective. An additional convolution with a 1 μm wide Gaussian profile gives a very good agreement with the measured values. The neccessity of the additional convolution is probably due to vibration of the detector.

the depth-of-focus of the optical system, which limits the maximal thickness of the luminescence screen, and spherical aberrations, since the microscope optic looks onto the luminescence screen through a supporting structure. All three limitations are a function of the numerical aperture NA of the system. Thus, it is important to find the optimal combination of numerical aperture, screen thickness and magnification.

4 Reconstruction

In order to maintain the high spatial resolution of the detector in the tomograms, the sampling theorem demands the recording of $\frac{\pi}{2}\frac{x}{\Delta x}$ images, where x is the size of the object and Δx is the resolution of the detector, i.e. 500–1000 projection images are required to obtain a resolution of better than 2 μm in the tomogram of a 500 μm object. These images are normalized to the white-field intensity to reduce artefacts due to beam- and detector inhomogenities. Remaining pixel inhomogenities, which lead to ring-artefacts in the reconstruction[12] are filtered out by a notch filter, which attenuates the values of the Fourier transform in the vertical axis in the sinogram prior to the tomographic reconstruction.[15] The tomograms are calculated with a filtered convoluted backprojection algorithm. Since outline mode enhanced edge contrast by a very narrow spaced pair of fringes, strike artefacts arise quite easily in the reconstruction at discontinuities, as the are produced by abrupt shifts in the movement of the rotation axis during the scan. This artefacts, which can degrade the image quality considerably, can be reduced by improving the mechanical stability of the system, although a numerical treatment of the shifted data seems to be possible, too. As a first test sample, we recorded 200 outline projections of a bundle of human hairs on high-resolution film over 180 degree of angle of view. Figure 6 shows a reconstructed cross-section of the three hairs with a spatial resolution of about 3 μm.

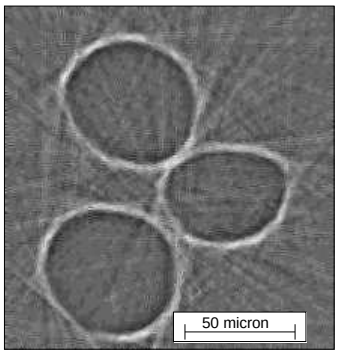

Figure 6: Tomographic reconstruction of three human hairs. 200 phase-contrast images were recorded in outline-mode on high resolution film.

5 Applications

In the following we are going to give some examples of applications of phase-contrast microtomography. In the frame of an international global reef monitioring program scientists are interested in the internal structure of foraminiferas from different seas in the world. Pathological abnormalities in the central structure, gives information about the environmental conditions the specimens were growing in. Although flat foraminiferas can be imaged easily in phase-contrast projection mode, spherical specimens had to be cut in thin slices and imaged seperately until now. Fig 7a shows a phase-contrast image of flat foraminifera, Fig 7b the tomographic reconstruction of a slice through a spherical specimen.

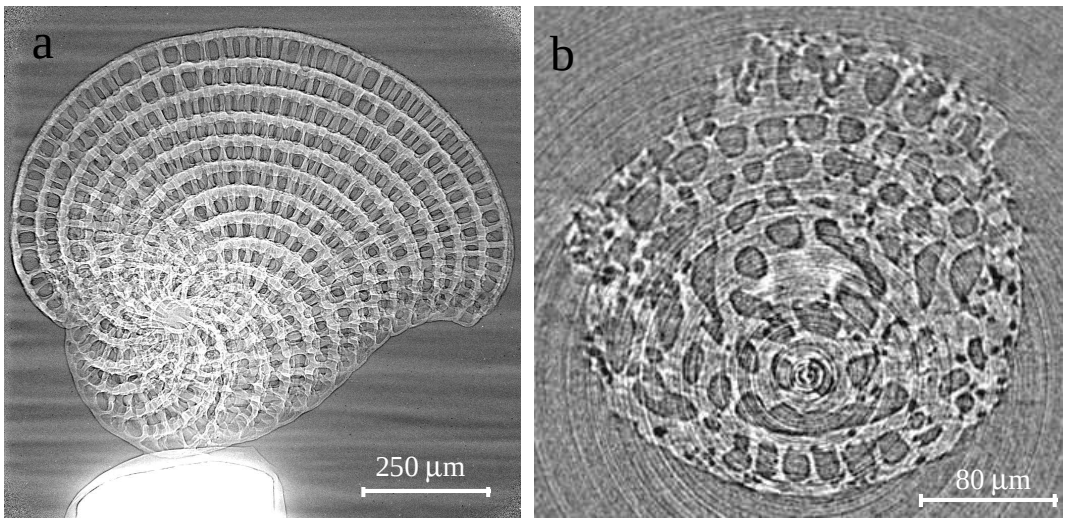

Figure 7: Phase-contrast images of two foraminifera specimen. a) Projection image of a flat foraminifera in 25 keV in 10 cm distance. b) Tomographic reconstruction of a spherical specimen from 500 projection at 25 keV and 10 cm distance. In both images the edge-enhancement effect of phase-contrast imaging is easily visible.

The second example is the image of a spider fang. Here the distribution of zinc and the inner structure of the fang are of interest. In Fig.8 a projection through the fang is shown at 20 keV in 6 cm distance. To reconstruct 3D information, 500 images were recorded over 180 degree, exposuretime at a undulator source (ID 22) at the ESRF was 500 msec. In the cross-sections (Fig. 9) the inner channel is visible as well as a bunch of very thin ($\emptyset \tilde{} 1 \mu m$) fibers or tubes around the inner channel. From reconstructing some 60 slices, a 3D rendering of the fang was made with the graphic package IDL on a HP workstation (Fig. 10).

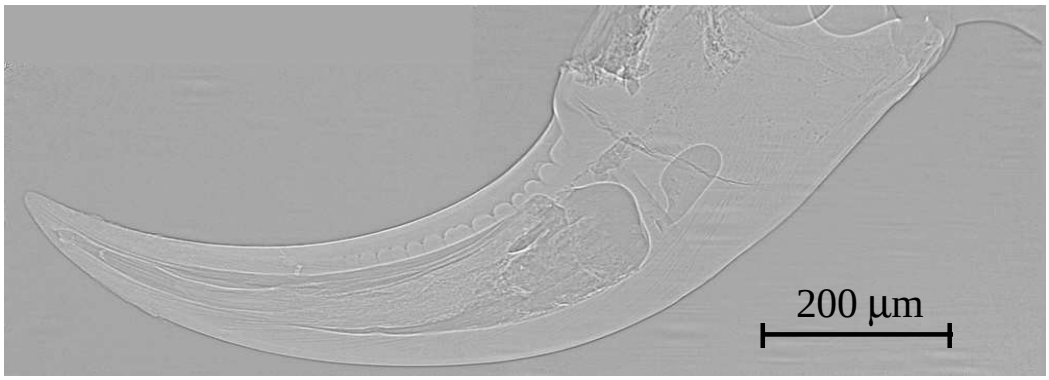

Figure 8: Phase-contrast image of a spider fang at 6 cm distance in a 20 keV beam.

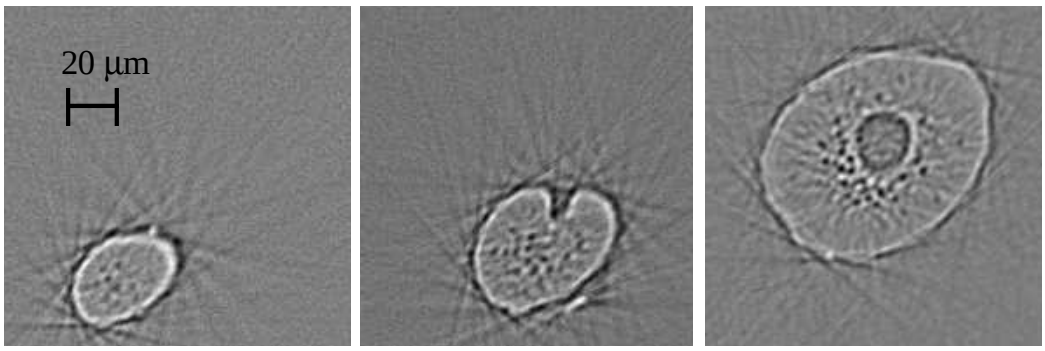

Figure 9: Three reconstructed cross-sections through the spider fang at 10, 15 and 90 μm from the tip. In the second image the exit of the inner channel is visible, in the third image a tubular structure around the channel. The stripe artefacts are due to undersampling in number of projections.

Conclusion

It is of particular interest to use phase-contrast tomography in medical applications like microscopy of biopsies and other tissue specimens, since for such samples radiation damage due to the absorbed dose often limits both, achievable contrast and spatial resolution. Outline mode tomography seem to be a promising extension to imaging applications in fields of research where the atomic composition differences between sample constituents do not allow e□cient absorption contrast imaging. One very well-suited application is the study of liquid-air interfaces which are of fundamental importance for several problems in soil science and have not been observed previously in realistic soil samples. Various applications can be seen in material science and biology, where samples have to be imaged in a natural

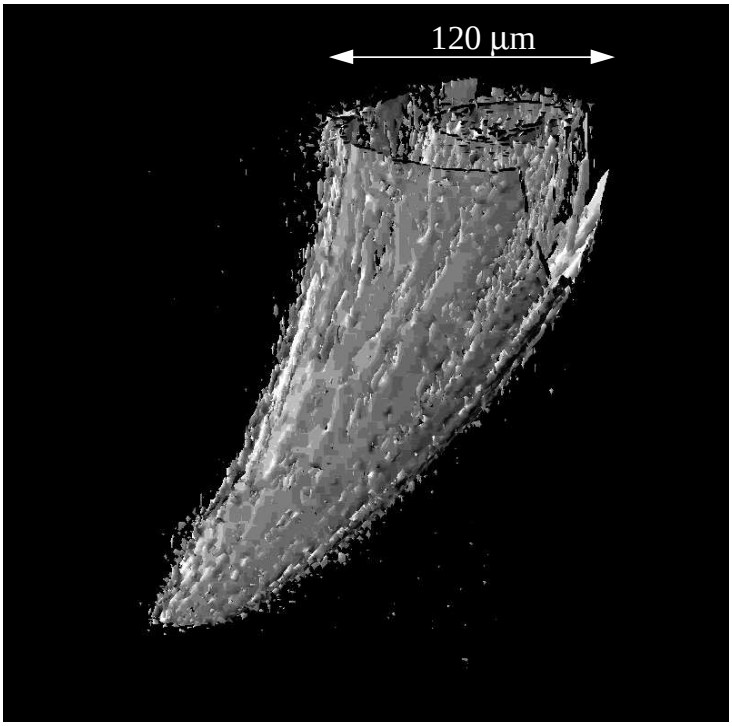

Figure 10: 3D rendering of the spider fang from 60 reconstructed cross-sections.

state without dyeing or drying or where three-dimensional information is needed with spatial resolution down to a micrometer.

Acknowledgments

We would like to thank P. Spanne for his help in the tomographic reconstruction, M. Pecheux (U. of Nice) and A. Thompson for their courtesy to provide the shown samples.

REFERENCES

[1] L. Grodzins. Optimum energies for x-ray transmission tomography of small samples. 206:541–546, 1983.

[2] A.C. Thompson, J. LLacer, et al. Computed tomography using synchrotron radiation. 222, 1984.

[3] W.S. Haddad, I. McNulty, J.E. Trebes, E.H. Anderson, R.A. Levesque, and L. Yang. Ultrahigh-resolution x-ray tomography. , 266:1213–1215, 1994.

[4] M.D. Silver. Towards a micrometer resolution x-ray tomographic microscope. , 2516:135–147, 1995.

[5] B.P. Flannery, H.W. Deckman, W.G. Roberge, and K.L. D'Amico. Three-dimensional x-ray microtomography. *Science*, pages 1439–1444, 1987.

[6] U. Bonse, Z. Johnson, M.Nichols, R. Nusshardt, S. Krasnicki, and J. Kinney. High resolution tomography with chemical specificity. A246:644–648, 1986.

[7] A. Snigirev. The recent development of bragg-fresnel crystal optics. experiments and applications at the esrf. 1995.

[8] A. Snigirev, I. Snigireva, V. Kohn, and S.M. Kuznetsov. On the requirements to the instrumentation for the new generation of the synchrotron radiation sources. beryllium windows. *Nucl. Instrum. Methods*, A 370:634–640, 1996.

[9] G. Schmahl and D. Rudolph. Proposal for a phase contrast x-ray microscope. In P.C. Cheng and G. J.Jan, editors, *X-Ray Microscopy*, Berlin, 1987. Springer.

[10] A. Momose, T. Takeda, Y. Itai, and K. Hirano. Phase-contrast x-ray computed tomography for oberserving biological soft tissues. , 2:473–475, 1996.

[11] C. Raven, A. Snigirev, I. Snigireva, P. Spanne, A. Souvorov, and V. Kohn. Phase-contrast microtomography with coherent high-energy synchrotron x rays. , 69:1826–1828, 1996.

[12] A. C. Kak and M. Slaney. *Principles of Computerized Tomographic Imaging*. IEEE press, New York, 1988.

[13] P. Cloetens, M. Pateyron-Salome, J.Y. Bu□ere, G. Peix, J. Baruchel, F. Peyrin, and M. Schlenker. Observation of microstructure and damage in materials by phase sensitive radiography and tomography. , 81:5878–5886, 1997.

[14] C. Raven, A. Koch, and A. Snigirev. X-ray computed tomography with micrometer spatial resolution. , 4:157, 1997.

[15] C. Raven. Removing ring-artefacts in tomographic reconstructions by fourier space filtering. , 1997.